

# Factor Graphs for Quantum Probabilities

August 3, 2015

Hans-Andrea Loeliger and Pascal O. Vontobel

**Abstract**—A factor-graph representation of quantum-mechanical probabilities (involving any number of measurements) is proposed. Unlike standard statistical models, the proposed representation uses auxiliary variables (state variables) that are not random variables. All joint probability distributions are marginals of some complex-valued function  $q$ , and it is demonstrated how the basic concepts of quantum mechanics relate to factorizations and marginals of  $q$ .

## I. INTRODUCTION

Factor graphs [2]–[6] and similar graphical notations [7]–[10] are widely used to represent statistical models with many variables. The graphical notation can be helpful in various ways, including the elucidation of the model itself and the derivation of algorithms for statistical inference.

In this paper, we show how quantum mechanical probabilities (including, in particular, joint distributions over several measurements) can be expressed in factor graphs that are fully compatible with factor graphs of standard statistical models. This is not trivial: despite being a statistical theory, quantum mechanics [11], [12] does not seem to fit into standard statistical categories; indeed, it has often been said that quantum mechanics is a generalization of probability theory that cannot be understood in terms of “classical” statistical modeling. Existing graphical representations of quantum mechanics such as Feynman diagrams [13], tensor diagrams [14], and quantum circuits [12, Chap. 4] do not explicitly represent probabilities, and they are not compatible with “classical” graphical models.

Therefore, this paper is not just about a graphical notation, but it offers a perspective of quantum mechanical probabilities that has not (as far as we know) been proposed before.

In order to introduce this perspective, recall that statistical models usually contain auxiliary variables (also called hidden variables or state variables), which are essential for factorizing the joint probability distribution. For example, a hidden Markov model with primary variables  $Y_1, \dots, Y_n$  is defined by a joint probability mass function of the form

$$p(y_1, \dots, y_n, x_0, \dots, x_n) = p(x_0) \prod_{k=1}^n p(y_k, x_k | x_{k-1}), \quad (1)$$

where  $X_0, X_1, \dots, X_n$  are auxiliary variables (hidden variables) that are essential for the factorization (1). More generally, the joint distribution  $p(y_1, \dots, y_n)$  of some primary

H.-A. Loeliger is with the Department of Information Technology and Electrical Engineering, ETH Zurich, Switzerland. Email: loeliger@isi.ee.ethz.ch.

P. O. Vontobel is with the Department of Information Engineering, The Chinese University of Hong Kong. Email: pascal.vontobel@ieee.org.

A much abbreviated version of this paper was presented at ISIT 2012 [1].

variables  $Y_1, \dots, Y_n$  is structured by a factorization of the joint distribution  $p(y_1, \dots, y_n, x_0, \dots, x_m)$  with auxiliary variables  $X_0, \dots, X_m$  and

$$p(y_1, \dots, y_n) = \sum_{x_0, \dots, x_m} p(y_1, \dots, y_n, x_0, \dots, x_m), \quad (2)$$

where the sum is over all possible values of  $X_0, \dots, X_m$ . (For the sake of exposition, we assume here that all variables have finite alphabets.) However, quantum-mechanical joint probabilities cannot, in general, be structured in this way.

We now generalize  $p(y_1, \dots, y_n, x_0, \dots, x_m)$  in (2) to an arbitrary complex-valued function  $q(y_1, \dots, y_n, x_0, \dots, x_m)$  such that

$$p(y_1, \dots, y_n) = \sum_{x_0, \dots, x_m} q(y_1, \dots, y_n, x_0, \dots, x_m). \quad (3)$$

The purpose of  $q$  is still to enable a nice factorization, for which there may now be more opportunities. Note that the concept of marginalization carries over to  $q$ ; in particular, all marginals of  $p(y_1, \dots, y_n)$  (involving any number of variables) are also marginals of  $q$ . However, the auxiliary variables  $X_0, \dots, X_m$  are not, in general, random variables, and marginals of  $q$  involving one or several of these variables are not, in general, probability distributions.

It may not be obvious that this generalization is useful, but we will show that it allows natural representations of quantum-mechanical probabilities involving any number of measurements.

This paper is not concerned with physics, but only with the peculiar joint probability distributions that arise in quantum mechanics. However, we will show how the basic concepts and terms of quantum mechanics relate to factorizations and marginals of suitable functions  $q$ . For the sake of clarity, we will restrict ourselves to finite alphabets (except in Appendix A), but this restriction is not essential. Within this limited scope, this paper may even be used as a self-contained introduction to quantum-mechanical probabilities.

To the best of our knowledge, describing quantum probabilities (and, indeed, any probabilities) by explicitly using a function  $q$  as in (3) is new. Nonetheless, this paper is, of course, related to much previous work in quantum mechanics and quantum computation. For example, quantum circuits as in [12, Chap. 4] have natural interpretations in terms of factor graphs as will be discussed in Section V-B. Our factor graphs are also related to tensor diagrams [14], cf. Section II-B. Also related is the very recent work by Mori [15]. On the other hand, quantum Bayesian networks (see, e.g., [16]) and quantum belief propagation (see, e.g., [17]) are

not immediately related to our approach since they are not based on (3) (and they lack Proposition 1 in Section II).

The paper is structured as follows. Section II reviews factor graphs and their connection to linear algebra. In Section III, we express elementary quantum mechanics (with a single projection measurement) in factor graphs; we also demonstrate how the Schrödinger picture, the Heisenberg picture, and even an elementary form of Feynman path integrals are naturally expressed in terms of factor graphs. Multiple and more general measurements are addressed in Section IV. Section V addresses partial measurements, decompositions of unitary operators (including quantum circuits), and the emergence of non-unitary operators from unitary interactions. In Section VI, we revisit measurements and briefly address their realization in terms of unitary interactions. Some additional remarks on the prior literature are given in Section VII. Section VIII concludes the paper.

In Appendix A, we briefly discuss the Wigner–Weyl representation, which leads to another factor graph representation. In Appendix B, we briefly address the extension of Monte Carlo methods to the factor graphs of this paper.

This paper contains many figures of factor graphs that represent some complex function  $q$  as in (3). The main figures are Figs. 12, 23, 36, and 45; in a sense, the whole paper is about explaining and exploring these four figures.

We will use standard linear algebra notation rather than the bra-ket notation of quantum mechanics. The Hermitian transpose of a complex matrix  $A$  will be denoted by  $A^H \triangleq \overline{A^T}$ , where  $A^T$  is the transpose of  $A$  and  $\overline{A}$  is the componentwise complex conjugate. An identity matrix will be denoted by  $I$ . The symbol “ $\propto$ ” denotes equality of functions up to a scale factor.

## II. ON FACTOR GRAPHS

### A. Basics

Factor graphs represent factorizations of functions of several variables. We will use Forney factor graphs<sup>1</sup> (also called normal factor graphs) as in [3]–[5], where nodes (depicted as boxes) represent factors and edges represent variables. For example, assume that some function  $f(x_1, \dots, x_5)$  can be written as

$$f(x_1, \dots, x_5) = f_1(x_1, x_2, x_5) f_2(x_2, x_3) f_3(x_3, x_4, x_5). \quad (4)$$

The corresponding factor graph is shown in Fig. 1.

In this paper, all variables in factor graphs take values in finite alphabets (except in Appendix A) and all functions take values in  $\mathbb{C}$ .

The factor graph of the hidden Markov model (1) is shown in Fig. 2. As in this example, variables in factor graphs are often denoted by capital letters.

The Forney factor-graph notation is intimately connected with the idea of opening and closing boxes [4]–[6]. Concerning

<sup>1</sup>Factor graphs as in [2] represent variables not by edges, but by variable nodes. Adapting Proposition 1 for such factor graphs is awkward.

Henceforth in this paper, “factor graph” means “Forney factor graph”; the qualifier “Forney” (or “normal”) will sometimes be added to emphasize that the distinction matters.

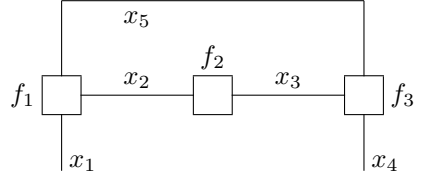


Fig. 1. Factor graph (i.e., Forney factor graph) of (4).

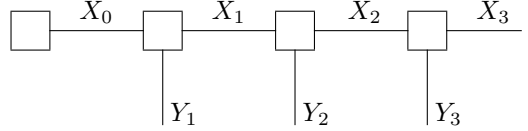


Fig. 2. Factor graph of the hidden Markov model (1) for  $n = 3$ .

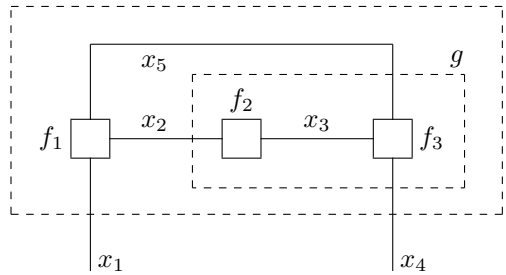


Fig. 3. Closing boxes in factor graphs.

the latter, consider the dashed boxes in Fig. 3. The *exterior function* of such a box is defined to be the product of all factors inside the box, summed over all its internal variables. The exterior function of the inner dashed box in Fig. 3 is

$$g(x_2, x_4, x_5) \triangleq \sum_{x_3} f_2(x_2, x_3) f_3(x_3, x_4, x_5), \quad (5)$$

and the exterior function of the outer dashed box is

$$f(x_1, x_4) \triangleq \sum_{x_2, x_3, x_5} f(x_1, \dots, x_5). \quad (6)$$

The summations in (5) and (6) range over all possible values of the corresponding variable(s).

*Closing a box* means replacing the box with a single node that represents the exterior function of the box. For example, closing the inner dashed box in Fig. 3 replaces the two nodes/factors  $f_2(x_2, x_3)$  and  $f_3(x_3, x_4, x_5)$  by the single node/factor (5); closing the outer dashed box in Fig. 3 replaces all nodes/factors in (4) by the single node/factor (6); and closing first the inner dashed box and then the outer dashed box replaces all nodes/factors in (4) by

$$\sum_{x_2, x_5} f_1(x_1, x_2, x_5) g(x_2, x_4, x_5) = f(x_1, x_4). \quad (7)$$

Note the equality between (7) and (6), which holds in general:

**Proposition 1.** Closing an inner box within some outer box (by summing over the internal variables of the inner box) does not change the exterior function of the outer box.  $\square$

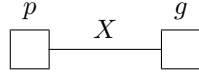


Fig. 4. Factor graph of  $E[g(X)]$  according to (8).

This simple fact is the pivotal property of Forney factor graphs. Closing boxes in factor graphs is thus compatible with marginalization both of probability mass functions and of complex-valued functions  $q$  as in (3), which is the basis of the present paper.

*Opening a box* in a factor graph means the reverse operation of expanding a node/factor into a factor graph of its own.

A *half edge* in a factor graph is an edge that is connected to only one node (such as  $x_1$  in Fig. 1). The *exterior function of a factor graph*<sup>2</sup> is defined to be the exterior function of a box that contains all nodes and all full edges, but all half edges stick out (such as the outer box in Fig. 3). For example, the exterior function of Fig. 1 is (6). The *partition sum*<sup>3</sup> of a factor graph is the exterior function of a box that contains the whole factor graph, including all half edges; the partition sum is a constant.

The exterior function of Fig. 2 is  $p(x_n, y_1, \dots, y_n)$ , and its partition sum equals one.

Factor graphs can also express expectations: the partition sum (and the exterior function) of Fig. 4 is

$$E[g(X)] = \sum_x p(x)g(x), \quad (8)$$

where  $p(x)$  is a probability mass function and  $g$  is an arbitrary real-valued (or complex-valued) function.

The equality constraint function  $f_=$  is defined as

$$f_=(x_1, \dots, x_n) = \begin{cases} 1, & \text{if } x_1 = \dots = x_n \\ 0, & \text{otherwise.} \end{cases} \quad (9)$$

The corresponding node (which is denoted by “=”) can serve as a branching point in a factor graph (cf. Figs. 19–22): only configurations with  $x_1 = \dots = x_n$  contribute to the exterior function of any boxes containing these variables.

A variable with a fixed known value will be marked by a solid square as in Figs. 10 and 21.

## B. Factor Graphs and Matrices

A matrix  $A \in \mathbb{C}^{m \times n}$  may be viewed as a function

$$\{1, \dots, m\} \times \{1, \dots, n\} \rightarrow \mathbb{C} : (x, y) \mapsto A(x, y). \quad (10)$$

The multiplication of two matrices  $A$  and  $B$  can then be written as

$$(AB)(x, z) = \sum_y A(x, y)B(y, z), \quad (11)$$

which is the exterior function of Fig. 5. Note that the identity matrix corresponds to an equality constraint function  $f_=(x, y)$ .

<sup>2</sup>What we here call the exterior function of a factor graph, is called *partition function* in [21]. The term “exterior function” was first used in [20].

<sup>3</sup>What we call here the partition sum has often been called *partition function*.

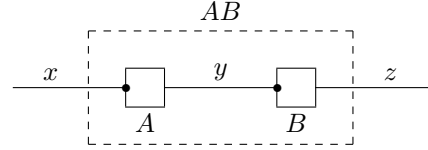


Fig. 5. Factor-graph representation of matrix multiplication (11). The small dot denotes the variable that indexes the rows of the corresponding matrix.

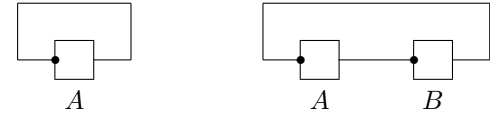


Fig. 6. Factor graph of  $\text{tr}(A)$  (left) and of  $\text{tr}(AB) = \text{tr}(BA)$  (right).

In this notation, the trace of a square matrix  $A$  is

$$\text{tr}(A) = \sum_x A(x, x), \quad (12)$$

which is the exterior function (and the partition sum) of the factor graph in Fig. 6 (left). Fig. 6 (right) shows the graphical proof of the identity  $\text{tr}(AB) = \text{tr}(BA)$ .

Factor graphs for linear algebra operations such as Fig. 5 and Fig. 6 (and the corresponding generalizations to tensors) are essentially tensor diagrams (or trace diagrams) as in [18], [19]. This connection between factor graphs and tensor diagrams was noted in [20]–[22].

## C. Reductions

Reasoning with factor graphs typically involves “local” manipulations of some nodes/factors (such as opening or closing boxes) that preserve the exterior function of all surrounding boxes. Some such reductions are shown in Figs. 7–10; these (very simple) reductions will be essential for understanding the proposed factor graphs for quantum-mechanical probabilities.

## D. Complex Conjugate Pairs

A general recipe for constructing complex functions  $q$  with real and nonnegative marginals as in (3) is illustrated in Fig. 11, where all factors are complex valued. Note that the lower dashed box in Fig. 11 mirrors the upper dashed box: all factors in the lower box are the complex conjugates of the corresponding factors in the upper dashed box. The exterior function of the upper dashed box is

$$g(y_1, y_2, y_3) \triangleq \sum_{x_1, x_2} g_1(x_1, y_1)g_2(x_1, x_2, y_2)g_3(x_2, y_3) \quad (13)$$

and the exterior function of the lower dashed box is

$$\sum_{x'_1, x'_2} \overline{g_1(x'_1, y_1)} \overline{g_2(x'_1, x'_2, y_2)} \overline{g_3(x'_2, y_3)} = \overline{g(y_1, y_2, y_3)}. \quad (14)$$

It follows that closing both boxes in Fig. 11 yields

$$\overline{g(y_1, y_2, y_3)g(y_1, y_2, y_3)} = |g(y_1, y_2, y_3)|^2, \quad (15)$$

which is real and nonnegative.

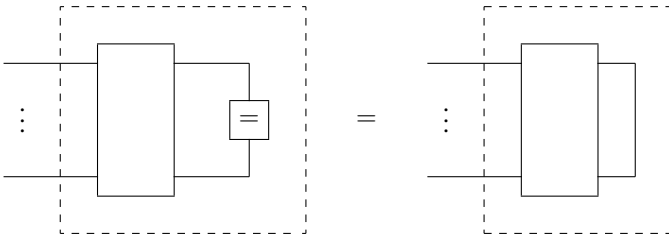


Fig. 7. A two-variable equality constraint (i.e., an identity matrix) can be dropped or added.

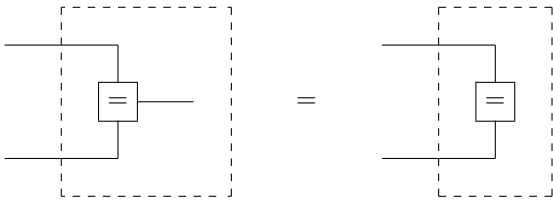


Fig. 8. A half edge out of an equality constraint node (of any degree) can be dropped or added.

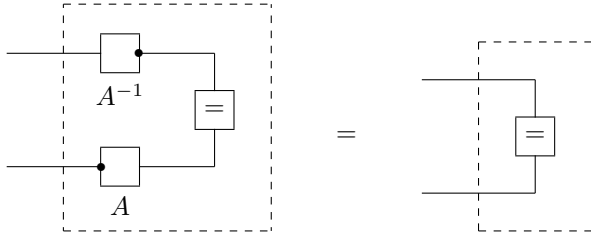


Fig. 9. A regular square matrix  $A$  multiplied by its inverse reduces to an identity matrix (i.e., a two-variable equality constraint).

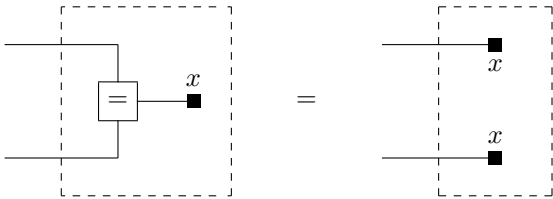


Fig. 10. A fixed known value (depicted as a small solid square) propagates through, and thereby eliminates, an equality constraint.

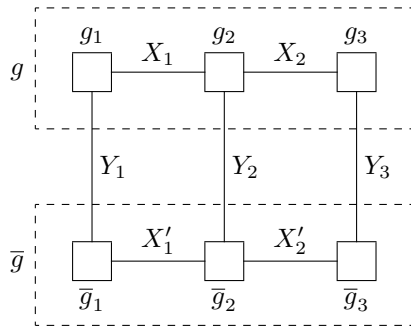


Fig. 11. Factor graph with complex factors and nonnegative real marginal (15).

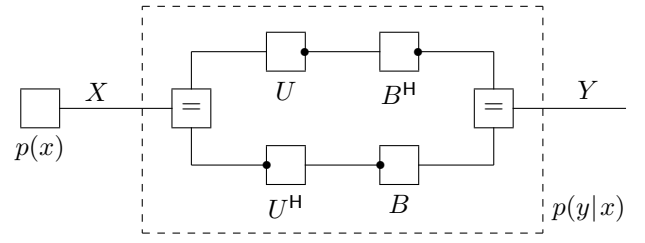


Fig. 12. Factor graph of an elementary quantum system.

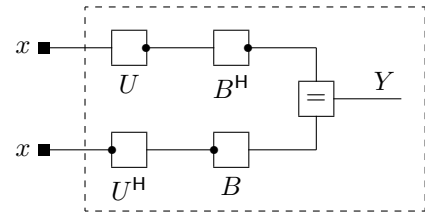


Fig. 13. Dashed box of Fig. 12 for fixed  $X = x$ . The partition sum of this factor graph equals one.

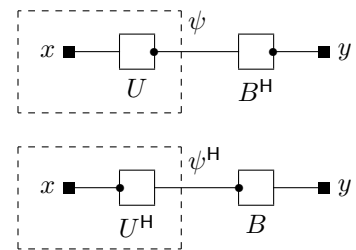


Fig. 14. Derivation of (17) and (18).

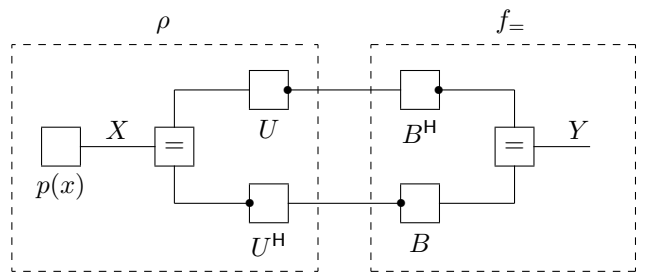


Fig. 15. Regrouping Fig. 12 into a density matrix  $\rho$  and an equality constraint.

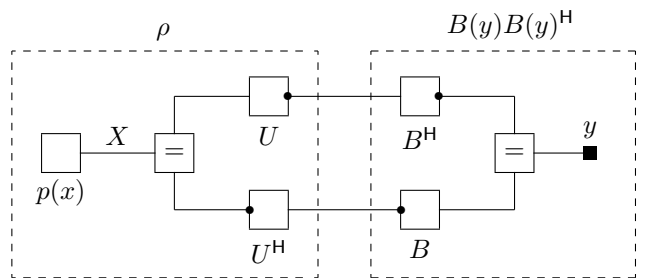


Fig. 16. Fig. 15 for fixed  $Y = y$ .

All factor graphs for quantum-mechanical probabilities that will be proposed in this paper (except in Appendix A) are special cases of this general form. With two parts that are complex conjugates of each other, such representations might seem redundant. Indeed, one of the two parts could certainly be *depicted* in some abbreviated form; however, as mathematical objects subject to Proposition 1, our factor graphs must contain both parts. (Also, the Monte Carlo methods of Appendix B work with samples where  $x'_k \neq x_k$ .)

### III. ELEMENTARY QUANTUM MECHANICS IN FACTOR GRAPHICS

#### A. Born's Rule

We begin with an elementary situation with a single measurement as shown in Fig. 12. In this factor graph,  $p(x)$  is a probability mass function,  $U$  and  $B$  are complex-valued unitary  $M \times M$  matrices, and all variables take values in the set  $\{1, \dots, M\}$ . The matrix  $U$  describes the unitary evolution of the initial state  $X$ ; the matrix  $B$  defines the measurement whose outcome is  $Y$ . The exterior function of the dashed box is  $p(y|x)$ , which we will examine below; with that box closed, the factor graph represents the joint distribution

$$p(x, y) = p(x)p(y|x). \quad (16)$$

We next verify that the dashed box in Fig. 12 can indeed represent a conditional probability distribution  $p(y|x)$ . For fixed  $X = x$ , this dashed box turns into (all of) Fig. 13 (see Fig. 10). By the reductions from Figures 8 and 9, closing the dashed box in Fig. 13 turns it into an identity matrix. It follows that the partition sum of Fig. 13 is  $I(x, x) = 1$  (i.e., the element in row  $x$  and column  $x$  of an identity matrix), thus complying with the requirement  $\sum_y p(y|x) = 1$ .

It is then clear from (16) that the partition sum of Fig. 12 equals 1.

For fixed  $X = x$  and  $Y = y$ , the dashed box in Fig. 12 turns into Fig. 14, and  $p(y|x)$  is the partition sum of that factor graph. The upper part of Fig. 14 evaluates to the scalar  $B(y)^H U(x)$ , where  $U(x)$  is column  $x$  of  $U$  and  $B(y)$  is column  $y$  of  $B$ ; the lower part of Fig. 14 evaluates to the scalar  $U(x)^H B(y)$ . The partition sum of Fig. 14 is the product of these two terms, i.e.,

$$p(y|x) = |B(y)^H U(x)|^2 \quad (17)$$

$$= |B(y)^H \psi|^2, \quad (18)$$

where  $\psi \triangleq U(x)$  is the quantum state (or the wave function).

With a little practice, the auxiliary Figures 13 and 14 need not actually be drawn and (17) can be directly read off Fig. 12.

#### B. Density Matrix

Consider Figures 15 and 16, which are regroupings of Fig. 12. The exterior function of the left-hand dashed box in these figures is the density matrix  $\rho$  of quantum mechanics, which can be decomposed into

$$\rho = \sum_x p(x)U(x)U(x)^H \quad (19)$$

and which satisfies

$$\text{tr}(\rho) = \sum_x p(x) \text{tr}(U(x)U(x)^H) \quad (20)$$

$$= \sum_x p(x) \text{tr}(U(x)^H U(x)) \quad (21)$$

$$= \sum_x p(x) \|U(x)\|^2 \quad (22)$$

$$= \sum_x p(x) \quad (23)$$

$$= 1. \quad (24)$$

The exterior function of the right-hand dashed box in Fig. 15 is an identity matrix (i.e., an equality constraint function), as is obvious from the reductions of Figs. 8 and 9. It is then obvious (cf. Fig. 6) that the partition sum of Fig. 15 is  $\text{tr}(\rho)$ , which equals 1 by (24). (But we already established in Section III-A that the partition sum of Figs. 12 and 15 is 1.)

The exterior function of the right-hand dashed box in Fig. 16 (with fixed  $Y = y$ ) is the matrix  $B(y)B(y)^H$ . From Fig. 12, we know that the partition sum of Fig. 16 is  $\sum_x p(x, y) = p(y)$ . Using Fig. 6, this partition sum can be expressed as

$$p(y) = \text{tr}(\rho B(y)B(y)^H) \quad (25)$$

$$= \text{tr}(B(y)^H \rho B(y)) \quad (26)$$

$$= B(y)^H \rho B(y). \quad (27)$$

Plugging (19) into (27) is, of course, consistent with (17).

#### C. Observables

In most standard formulations of quantum mechanics, the outcome of a physical experiment is not  $Y$  as in Fig. 12, but some (essentially arbitrary) real-valued function  $g(Y)$ .

In Fig. 17, we have augmented Fig. 12 by a corresponding factor  $g(Y)$ . The partition sum of Fig. 17 is thus

$$\text{E}[g(Y)] = \sum_y p(y)g(y), \quad (28)$$

cf. Fig. 4. Regrouping Fig. 17 as in Fig. 16 yields Fig. 18, the partition sum of which is

$$\text{E}[g(Y)] = \text{tr}(\rho O), \quad (29)$$

where the matrix  $O$  is the right-hand dashed box in Fig. 16. Note that, by the spectral theorem, an arbitrary Hermitian matrix  $O$  can be represented as in Fig. 18 and  $g(1), \dots, g(M)$  are the eigenvalues of  $O$ .

In this paper, however, we will focus on probabilities and we will not further use such expectations.

#### D. Evolution over Time: Schrödinger, Heisenberg, Feynman

Consider the factor graph of Fig. 19, which agrees with Fig. 12 except that the matrix  $U$  is expanded into the product  $U = U_n \cdots U_1$ . One interpretation of this factor graph is that the initial state  $X$  evolves unitarily over  $n$  discrete time steps until it is measured by a projection measurement as in Fig. 12. Note that a continuous-time picture may be obtained, if desired, by a suitable limit with  $n \rightarrow \infty$ .

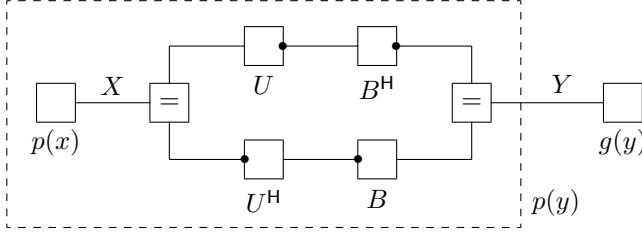


Fig. 17. Factor graph of expectation (28).

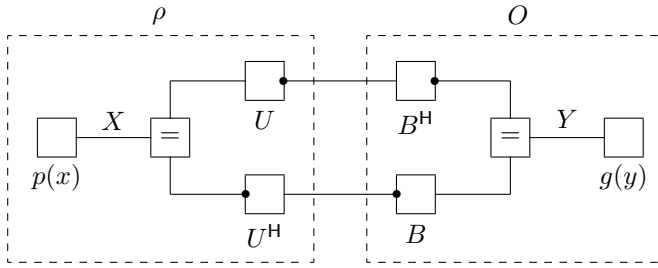


Fig. 18. Factor graph of expectation (29) with general Hermitian matrix  $O$ .

In this setting, the so-called Schrödinger and Heisenberg pictures correspond to sequentially closing boxes (from the innermost dashed box to the outermost dashed box) as in Figures 20 and 22, respectively; the former propagates the quantum state  $\psi$  (or the density matrix  $\rho$ ) forward in time while the latter propagates the measurement backwards in time. The resulting probability distribution over  $Y$  is identical by Proposition 1.

Both the Schrödinger picture and the Heisenberg picture can be reduced to sum-product message passing in a cycle-free graph as follows. In the Schrödinger picture, assume first that the initial state  $X$  is known. In this case, we obtain the cycle-free factor graph of Fig. 21, in which  $p(y)$  is easily computed by left-to-right sum-product message passing (cf. [2], [4]), which amounts to a sequence of matrix-times-vector multiplications

$$\psi_k = U_k \psi_{k-1} \quad (30)$$

with  $\psi_1 \triangleq U_1(x)$  (= column  $x$  of  $U_1$ ). The quantities  $\psi_1, \dots, \psi_n$  in Fig. 21 are the wave functions propagated up to the corresponding time. Since Fig. 21 consists of two complex conjugate parts, it suffices to carry out these computations for one of the two parts.

If the initial state  $X$  is not known, we write

$$p(y) = \sum_x p(x) p(y|x), \quad (31)$$

and each term  $p(y|x)$  can be computed as in Fig. 21. This decomposition carries over to the relation

$$\rho_k(x', x'') = \sum_x p(x) \psi_k(x') \psi_k^H(x'') \quad (32)$$

$$= \sum_x p(x) \psi_k(x') \overline{\psi_k(x'')} \quad (33)$$

between the wave function  $\psi_k$  and the density matrix  $\rho_k$  (see Figures 20 and 21) for  $k = 1, \dots, n$ .

In the Heisenberg picture (Fig. 22), we can proceed analogously. For any fixed  $Y = y$ , this value can be plugged into the factors/matrices  $B$  and  $B^H$ , which turns Fig. 22 into a cycle-free factor graph that looks almost like a time-reversed version of Fig. 21. In consequence,  $p(y)$  can be computed by right-to-left sum-product message passing, which again amounts to a sequence of matrix-times-vector multiplications.

Finally, we note that the dashed boxes in Fig. 19 encode Feynman's path integral in its most elementary embodiment. Each internal configuration (i.e., an assignment of values to all variables) in such a box may be viewed as a "path", and the corresponding product of all factors inside the box may be viewed as the (complex) weight of the path. The exterior function of the box is (by definition) the sum, over all internal configurations/paths, of the weight of each configuration/path.

#### IV. MULTIPLE AND MORE GENERAL MEASUREMENTS

We now turn to multiple and more general measurements. Consider the factor graph of Fig. 23. In this figure,  $U_0$  and  $U_1$  are  $M \times M$  unitary matrices, and all variables except  $Y_1$  and  $Y_2$  take values in the set  $\{1, \dots, M\}$ . The two large boxes in the figure represent measurements, as will be detailed below. The factor/box  $p(x_0)$  is a probability mass function over the initial state  $X_0$ . We will see that this factor graph (with suitable modeling of the measurements) represents the joint probability mass function  $p(y_1, y_2)$  of a general  $M$ -dimensional quantum system with two observations  $Y_1$  and  $Y_2$ . The generalization to more observed variables  $Y_1, Y_2, \dots$  is obvious.

The unitary matrix  $U_0$  in Fig. 23 represents the development of the system between the initial state and the first measurement according to the Schrödinger equation; the unitary matrix  $U_1$  in Fig. 23 represents the development of the system between the two measurements.

In the most basic case, the initial state  $X_0 = x_0$  is known and the measurements look as shown in Fig. 24, where the matrices  $B_1$  and  $B_2$  are also unitary (cf. Fig. 12). In this case, the observed variables  $Y_1$  and  $Y_2$  take values in  $\{1, \dots, M\}$  as well. Note that the lower part of this factor graph is the complex conjugate mirror of the upper part (as in Fig. 11).

In quantum-mechanical terms, measurements as in Fig. 24 are projection measurements with one-dimensional eigenspaces (as in Section III).

A very general form of measurement is shown in Fig. 27. In this case, the range of  $Y_k$  is a finite set  $\mathcal{Y}_k$ , and for each  $y_k \in \mathcal{Y}_k$ , the factor  $A_k(\tilde{x}_k, x_k, y_k)$  corresponds to a complex square matrix  $A_k(y_k)$  (with row index  $\tilde{x}_k$  and column index  $x_k$ ) such that

$$\sum_{y_k \in \mathcal{Y}_k} A_k(y_k)^H A_k(y_k) = I, \quad (34)$$

cf. [12, Chap. 2]. A factor-graphic interpretation of (34) is given in Fig. 28. Measurements as in Fig. 24 are included as a special case with  $\mathcal{Y}_k = \{1, \dots, M\}$  and

$$A_k(y_k) = A_k(y_k)^H = B_k(y_k) B_k(y_k)^H, \quad (35)$$

where  $B_k(y_k)$  denotes the  $y_k$ -th column of  $B_k$ . Note that, for fixed  $y_k$ , (35) is a projection matrix. Measurements will further be discussed in sections V-A and VI.

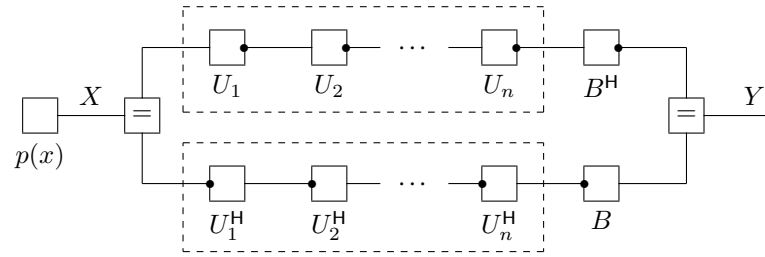


Fig. 19. Elementary quantum mechanics: unitary evolution over time in  $n$  steps followed by a single projection measurement.

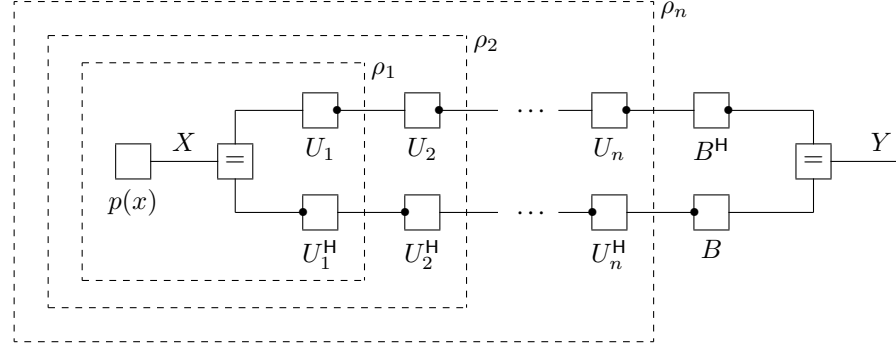


Fig. 20. Schrödinger picture.

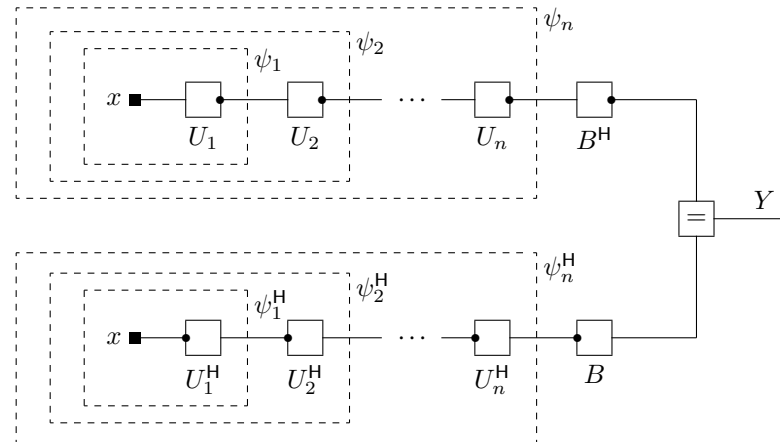


Fig. 21. Schrödinger picture with known initial state  $X = x$  and unitarily evolving quantum state (or wave function)  $\psi$ .

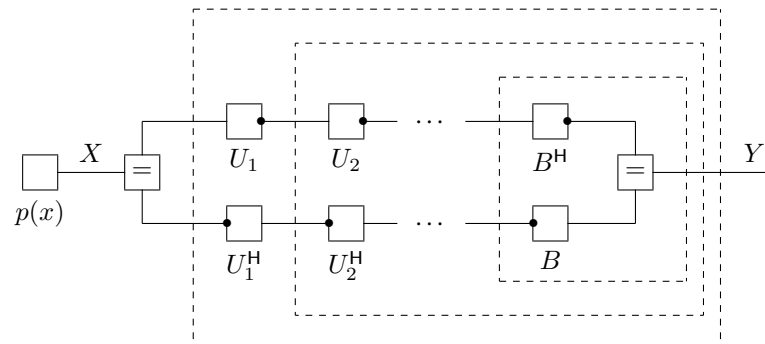


Fig. 22. Heisenberg picture.

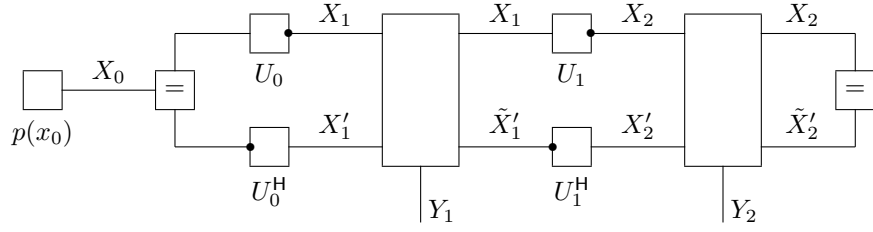


Fig. 23. Factor graph of a quantum system with two measurements and the corresponding observations  $Y_1$  and  $Y_2$ .

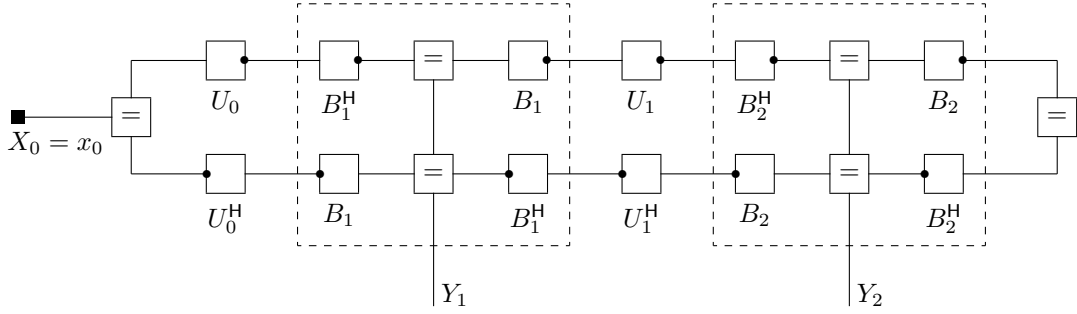


Fig. 24. Important special case of Fig. 23: all matrices are unitary and the initial state  $X_0 = x_0$  is known. In quantum-mechanical terms, such measurements are projection measurements with one-dimensional eigenspaces.

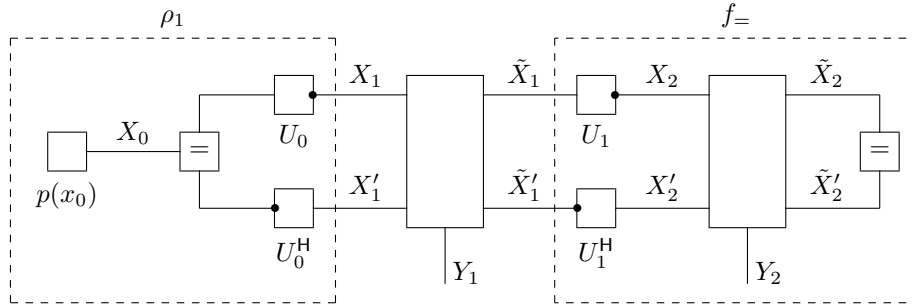


Fig. 25. The exterior function of the dashed box on the left is the density matrix  $\rho_1(x_1, x'_1)$ . The exterior function of the dashed box on the right is  $f_=(\tilde{x}_1, \tilde{x}'_1)$  (assuming that  $Y_2$  is unknown).

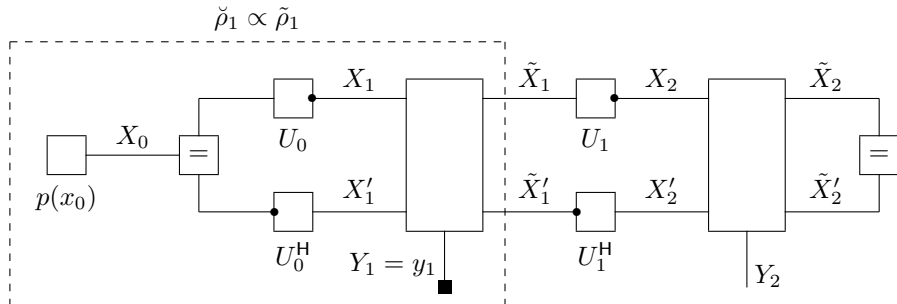


Fig. 26. The exterior function of the dashed box  $\check{\rho}_1$  equals the density matrix  $\tilde{\rho}_1$ , up to a scale factor, after measuring  $Y_1 = y_1$ , cf. (39).

It is clear from Section II-D that the exterior function of Fig. 23 (with measurements as in Fig. 24 or as in Fig. 27) is real and nonnegative. We now proceed to analyze these factor graphs and to verify that they yield the correct quantum-mechanical probabilities  $p(y_1, y_2)$  for the respective class of measurements. To this end, we need to understand the exterior functions of the dashed boxes in Fig. 25. We begin with the dashed box on the right-hand side of Fig. 25.

**Proposition 2 (Don't Mind the Future).** Closing the dashed box on the right-hand side in Fig. 25 (with a measurement as in Fig. 24 or as in Fig. 27, but with unknown result  $Y_2$  of the measurement) reduces it to an equality constraint function.  $\square$

**Proof:** For measurements as in Fig. 24, the proof amounts to a sequence of reductions according to Figs. 8 and 9, as illustrated in Fig. 29.

For measurements as in Fig. 27, the key step is the reduction of Fig. 28 to an equality constraint, which is equivalent to the condition (34).  $\square$

Proposition 2 guarantees, in particular, that a future measurement (with unknown result) does not influence present or past observations. The proposition clearly holds also for the extension of Fig. 23 to any finite number of measurements  $Y_1, Y_2, \dots$  and can then be applied recursively from right to left.

We pause here for a moment to emphasize this point: it is obvious from Figs. 23 and 24 (generalized to  $n$  measurements  $Y_1, \dots, Y_n$ ) that, in general, a measurement resulting in some variable  $Y_k$  affects the joint distribution of all other variables  $Y_1, \dots, Y_n$  (both past and future) *even if the result  $Y_k$  of the measurement is not known*. By Proposition 2, however, the joint distribution of  $Y_1, \dots, Y_{k-1}$  is not affected by the measurement of  $Y_k, \dots, Y_n$  provided that no measurement results are known.

**Proposition 3 (Proper Normalization).** The factor graph of Fig. 23 (with measurements as in Fig. 24 or as in Fig. 27) represents a properly normalized probability mass function, i.e., the exterior function  $p(y_1, y_2)$  is real and nonnegative and  $\sum_{y_1, y_2} p(y_1, y_2) = 1$ .  $\square$

In particular, the partition sum of Fig. 23 equals 1. Again, the proposition clearly holds also for the extension of Fig. 23 to any finite number of measurements  $Y_1, Y_2, \dots$

**Proof of Proposition 3:** Apply reductions according to Proposition 2 recursively from right to left in Fig. 23, followed by the final reduction  $\sum_{x_0} p(x_0) = 1$ .  $\square$

Consider now the dashed boxes on the left in Figs. 25 and 26, which correspond to the density matrix before and after measuring  $Y_1$ , respectively. A density matrix  $\rho$  is defined to be properly normalized if

$$\text{tr}(\rho) = 1. \quad (36)$$

The dashed box left in Fig. 25 is properly normalized ( $\text{tr}(\rho_1) = 1$ ) by (24). Proper normalization of  $\rho_k$  for  $k > 1$  follows from Propositions 5–7 below.

Consider next the dashed box in Fig. 26, which we will call  $\check{\rho}_1$ ; it is not a properly normalized density matrix:

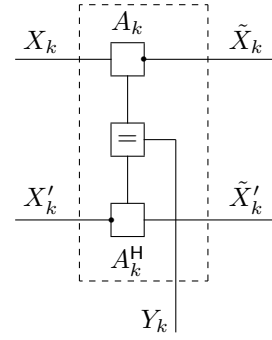


Fig. 27. General measurement as in [12, Chap. 2]. Condition (34) must be satisfied.

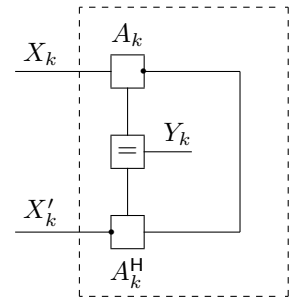


Fig. 28. The dashed box reduces to an equality constraint (i.e., an identity matrix) if and only if (34) holds.

**Proposition 4 (Trace of the Past).**

$$\text{tr}(\check{\rho}_1) = p(y_1); \quad (37)$$

more generally, with  $k$  measurements  $Y_1 = y_1, \dots, Y_k = y_k$  inside the dashed box, we have

$$\text{tr}(\check{\rho}_k) = p(y_1, \dots, y_k). \quad (38)$$

The proof is immediate from Propositions 2 and 3 (generalized to an arbitrary number of measurements). The properly normalized post-measurement density matrix is then

$$\tilde{\rho}_k \triangleq \check{\rho}_k / p(y_1, \dots, y_k). \quad (39)$$

**Proposition 5 (Unitary Evolution Between Measurements).**

The matrix  $\rho_{k+1}$  is obtained from the matrix  $\tilde{\rho}_k$  as

$$\rho_{k+1} = U_k \tilde{\rho}_k U_k^H. \quad (40)$$

The proof is immediate from Fig. 5. Note that  $\rho_{k+1}$  is properly normalized (provided that  $\tilde{\rho}_k$  is so).

**Proposition 6 (Basic Projection Measurement).** In Fig. 23 (generalized to any number of observations), if  $Y_k$  is measured as in Fig. 24, then

$$\begin{aligned} P(Y_k = y_k \mid Y_{k-1} = y_{k-1}, \dots, Y_1 = y_1) \\ = B_k(y_k)^H \rho_k B_k(y_k) \end{aligned} \quad (41)$$

$$= \text{tr}(\rho_k B_k(y_k) B_k(y_k)^H), \quad (42)$$

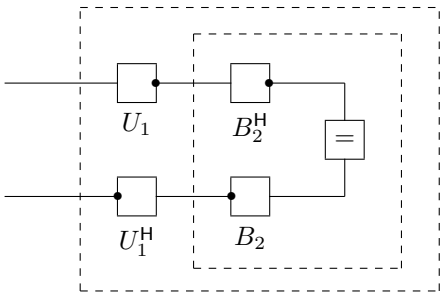
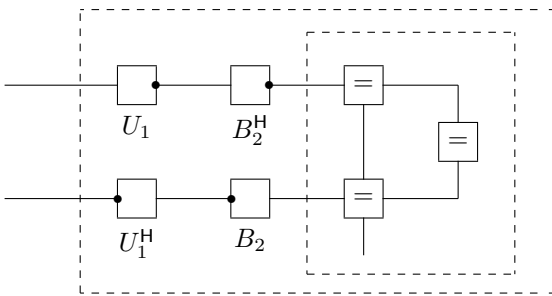
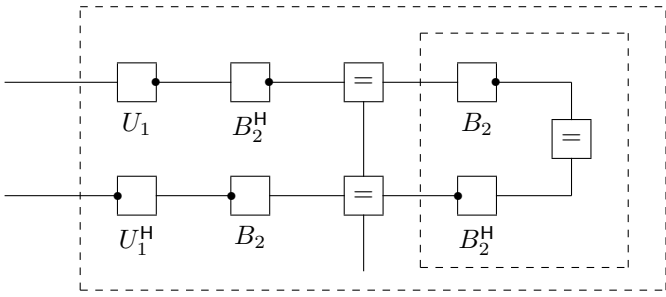


Fig. 29. Proof of Proposition 2 for measurements as in Fig. 24 by a sequence of reductions as in Figs. 9 and 8.

where  $B_k(y)$  is the  $y$ -th column of  $B_k$ . After measuring/observing  $Y_k = y_k$ , the density matrix is

$$\rho_k = B_k(y_k)B_k(y_k)^H. \quad (43)$$

□

Note that (43) is properly normalized because  $\text{tr}(B_k(y_k)B_k(y_k)^H) = \text{tr}(B_k(y_k)^H B_k(y_k)) = \|B_k(y_k)\|^2 = 1$ .

**Proof of Proposition 6:** For fixed  $y_1, \dots, y_{k-1}$ , we have

$$\begin{aligned} P(Y_k = y_k \mid Y_{k-1} = y_{k-1}, \dots, Y_1 = y_1) \\ \propto p(y_k, y_{k-1}, \dots, y_1), \end{aligned} \quad (44)$$

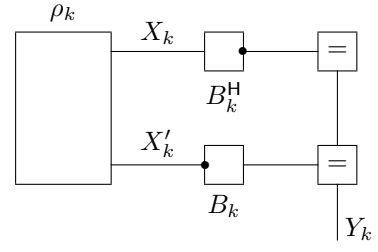


Fig. 30. Proof of Proposition 6: the exterior function equals (41) and (42).

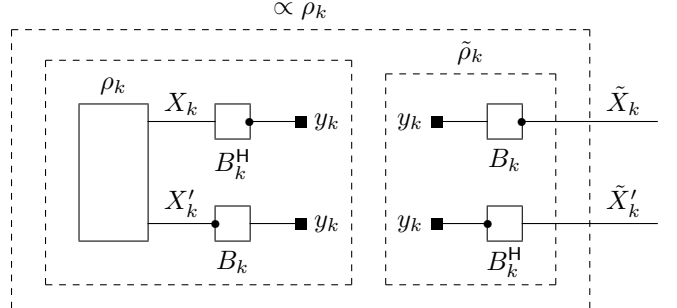


Fig. 31. Proof of Proposition 6: post-measurement density matrix  $\tilde{\rho}_k$ .

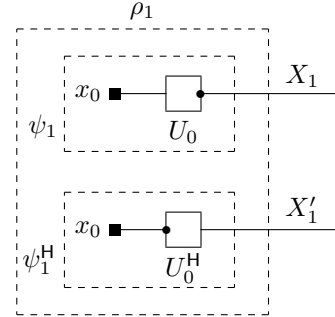


Fig. 32. Quantum state  $\psi_1$ .

where  $p$  is the exterior function of Fig. 23 (generalized to any number of observations and with measurements as in Fig. 24). We now reduce Fig. 23 to Fig. 30 as follows: everything to the right of  $Y_k$  reduces to an equality constraint according to Proposition 2 (see also Fig. 29), while everything before the measurement of  $Y_k$  (with  $Y_{k-1} = y_{k-1}, \dots, Y_1 = y_1$  plugged in) is subsumed by  $\rho_k$ . Note that the partition sum of Fig. 30 is  $\text{tr}(\rho_k) = 1$  (cf. Fig. 15), which means that the exterior function of Fig. 30 equals  $p(y_k \mid y_{k-1}, \dots, y_1)$ , i.e., the missing scale factor in (44) has been compensated by the normalization of  $\rho_k$ .

For any fixed  $Y_k = y_k$ , we can then read (41) and (42) from Fig. 30 (cf. Fig. 16). □

We now turn to the post-measurement density matrix  $\tilde{\rho}_k$ . For a measurement  $Y_k = y_k$  as in Fig. 24, the dashed box in Fig. 26 looks as in Fig. 31, which decomposes into two unconnected parts as indicated by the two inner dashed boxes. The exterior function of the left-hand inner dashed box in Fig. 31 is the constant (41); the right-hand inner dashed box equals (43). □

In the special case of Fig. 24, with known initial state

$X_0 = x_0$ , the matrix  $\rho_k$  factors as

$$\rho_k(x_k, x'_k) = \psi_k(x_k) \overline{\psi_k(x'_k)}, \quad (45)$$

or, in matrix notation,

$$\rho_k = \psi_k \psi_k^H, \quad (46)$$

where  $\psi_k$  is a column vector of norm 1. For  $k = 1$ , we have  $\psi_1(x_1) = U_0(x_1, x_0)$ , as shown in Fig. 32. The post-measurement density matrix  $\tilde{\rho}_k$  factors analogously, as is obvious from (43) or from Fig. 31. In quantum-mechanical terms,  $\psi_k$  is the quantum state (cf. Section III). The probability (41) can then be expressed as

$$P(Y_k = y \mid Y_{k-1} = y_{k-1}, \dots, Y_1 = y_1) = B_k(y)^H \psi_k \psi_k^H B_k(y) \quad (47)$$

$$= \|B_k(y)^H \psi_k\|^2. \quad (48)$$

**Proposition 7 (General Measurement).** In Fig. 23 (generalized to any number of observations), if  $Y_k$  is measured as in Fig. 27, then

$$P(Y_k = y_k \mid Y_{k-1} = y_{k-1}, \dots, Y_1 = y_1) = \text{tr}(A_k(y_k) \rho_k A_k(y_k)^H). \quad (49)$$

After measuring/observing  $Y_k = y_k$ , the density matrix is

$$\tilde{\rho}_k = \frac{A_k(y_k) \rho_k A_k(y_k)^H}{\text{tr}(A_k(y_k) \rho_k A_k(y_k)^H)} \quad (50)$$

□

**Proof:** The proof is parallel to the proof of Proposition 6. For fixed  $y_{k-1}, \dots, y_1$ , we have

$$P(Y_k = y_k \mid Y_{k-1} = y_{k-1}, \dots, Y_1 = y_1) \propto p(y_k, y_{k-1}, \dots, y_1), \quad (51)$$

where  $p$  is the exterior function of Fig. 23 (generalized to any number of observations and with measurements as in Fig. 27). We now reduce Fig. 23 to Fig. 33 as follows: everything to the right of  $Y_k$  reduces to an equality constraint while everything before the measurement of  $Y_k$  (with  $Y_{k-1} = y_{k-1}, \dots, Y_1 = y_1$  plugged in) is subsumed by  $\rho_k$ . From Fig. 28, we see that the partition sum of Fig. 33 is  $\text{tr}(\rho_k) = 1$ , which means that the exterior function of Fig. 33 equals  $p(y_k \mid y_{k-1}, \dots, y_1)$ , i.e., the missing scale factor in (51) has been compensated by the normalization of  $\rho_k$ .

For fixed  $Y_k = y_k$ , (49) is then obvious from Fig. 34.

Concerning the post-measurement density matrix  $\tilde{\rho}_k$ , for a measurement  $Y_k = y_k$  as in Fig. 27, the dashed box in Fig. 26 looks as in Fig. 35. The numerator of (50) is then obvious from Fig. 35, and the denominator of (50) is simply the proper normalization (36). □

In summary, Propositions 2–7 verify that the factor graph of Fig. 23 (with measurements as in Fig. 24 or as in Fig. 27) yields the correct quantum-mechanical probabilities for the respective class of measurements.

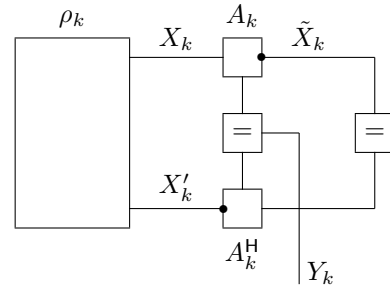


Fig. 33. Proof of Proposition 7: normalization.

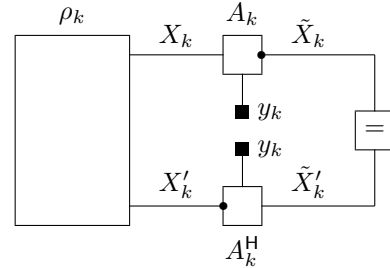


Fig. 34. Proof of Proposition 7: probability (49).

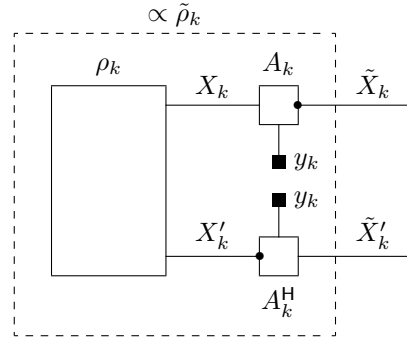


Fig. 35. Proof of Proposition 7: post-measurement density matrix  $\tilde{\rho}_k$ .

## V. DECOMPOSITIONS AND QUANTUM CIRCUITS, AND NON-UNITARY OPERATORS FROM UNITARY INTERACTIONS

Figs. 23 and 27, while fully general, do not do justice to the richness of quantum-mechanical probabilities and their factor-graphical representation, which we are now going to address.

### A. Decompositions and Partial Measurements

Consider the factor graph of Fig. 36. The following points are noteworthy. First, we note that the unitary matrices  $U_0, U_1, U_2$  in Fig. 36 have more than two incident edges. This is to be understood as illustrated in Fig. 37, where the rows of some matrix are indexed by  $X$  while its columns are indexed by the pair  $(V, W)$ . More generally, rows (marked by a dot) and columns may both be indexed by several variables. Note that, in this way, bundling two unconnected matrices as in Fig. 38 represents the tensor product  $A \otimes B$ . In Fig. 36, all matrices are square, which implies that the product of the alphabet sizes of the row-indexing variables must equal the product of the alphabet sizes of the column-indexing variables.

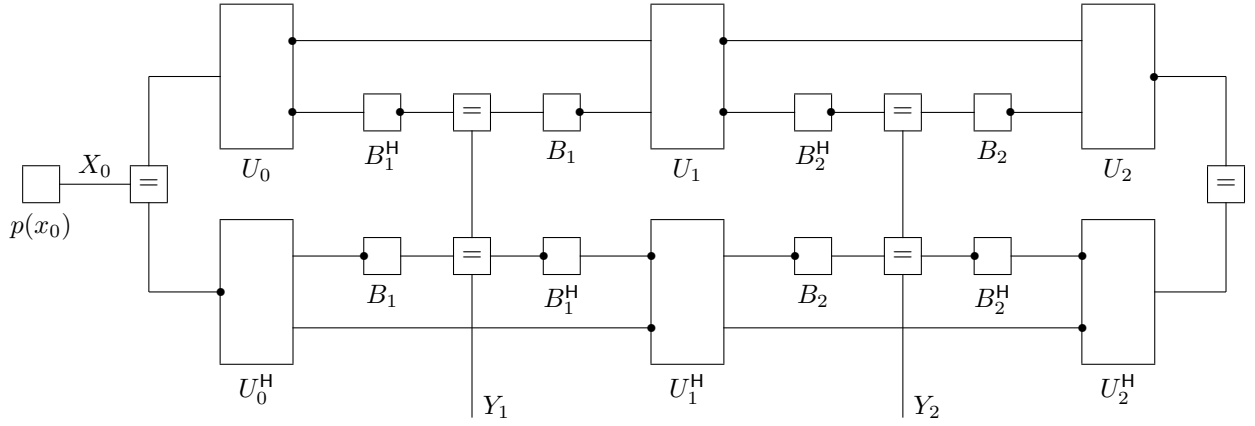


Fig. 36. Factor graph of a quantum system with partial measurements.

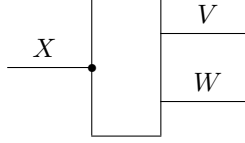


Fig. 37. Matrix with row index  $X$  and columns indexed by the pair  $(V, W)$ . (E.g.,  $X$  takes values in  $\{0, 1, 2, 3\}$  while  $V$  and  $W$  are both binary.)

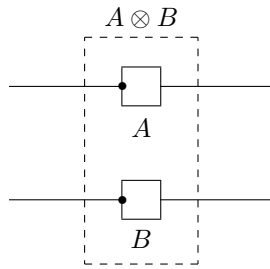


Fig. 38. Tensor product of matrices  $A$  and  $B$ .

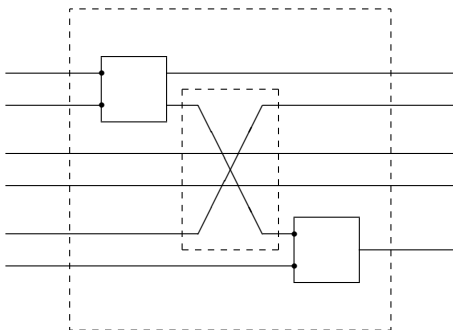


Fig. 39. Decomposition of a unitary matrix into smaller unitary matrices. Line switching as in the inner dashed box is itself a unitary matrix, cf. Fig. 42.

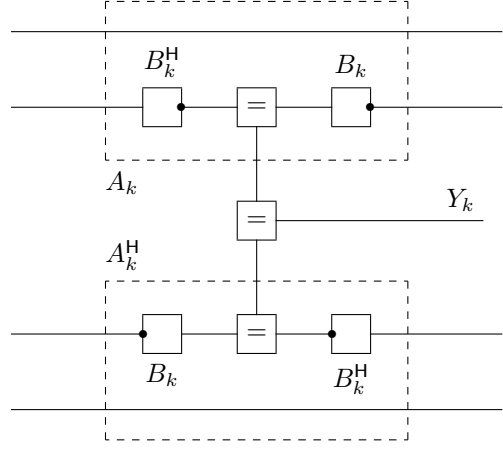


Fig. 40. Measurements in Fig. 36 as a special case of Fig. 27.

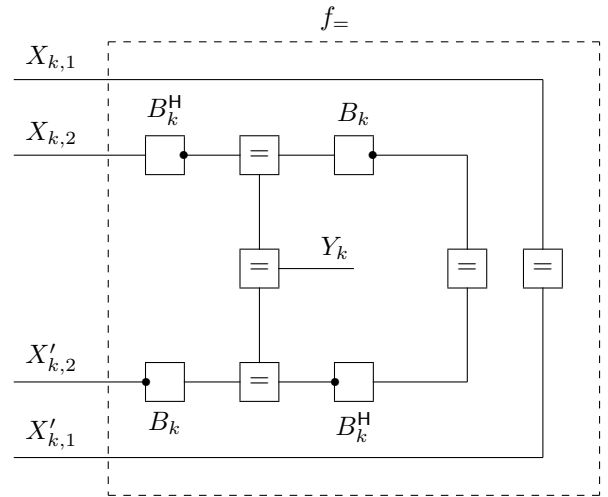


Fig. 41. The exterior function of the dashed box is  $f_=(x_{k,1}, x_{k,2}, x'_{k,2}) = f_=(x_{k,1}, x'_{k,1}) f_=(x_{k,2}, x'_{k,2})$ .

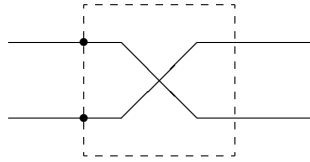


Fig. 42. Swap gate.

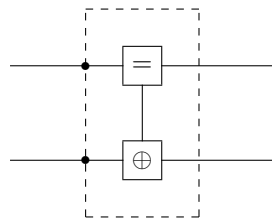


Fig. 43. Controlled-NOT gate.

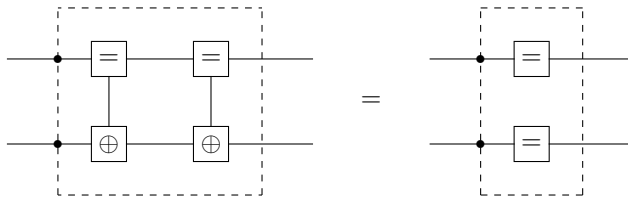


Fig. 44. Proof that Fig. 43 is unitary: the exterior functions left and right are equal.

Second, each edge in the factor graph of Fig. 36 may actually represent several (finite-alphabet) variables, bundled into a single compound variable.

Third, each of the unitary matrices  $U_0, U_1, U_2, \dots$  may itself be a product, either of smaller unitary matrices as illustrated in Fig. 39, or of more general factors as exemplified by Fig. 43; see also Section V-B below.

Forth, it is obvious from Fig. 36 that each measurement involves only some of the variables while some other variables are left alone. The actual measurements shown in Fig. 36 are as in Fig. 24 (with unitary matrices  $B_1, B_2 \dots$ ), but more general measurements could be used.

The measurements in Fig. 36 (including the uninvolved variables) are indeed a special case of measurements as in Fig. 27, as is obvious from Fig. 40, from where we may also read  $A_k(y_k) = I \otimes (B_k(y_k)B_k(y_k)^\text{H})$ . In order to verify (34), we first recall its factor-graphic interpretation in Fig. 28, which, in this case, amounts to the obvious reduction of Fig. 41 to an equality constraint.

### B. Quantum Circuits

Quantum gates [12, Chap. 4] are unitary matrices used in quantum computation. (In Figs. 23 or 36, such quantum gates would appear as, or inside,  $U_0, U_1, U_2, \dots$ ) For example, Fig. 42 shows a swap gate and Fig. 43 shows a controlled-NOT gate in factor-graph notation. All variables in these two examples are  $\{0, 1\}$ -valued (rather than  $\{1, 2\}$ -valued), both rows and columns are indexed by pairs of bits (cf. Fig. 37),

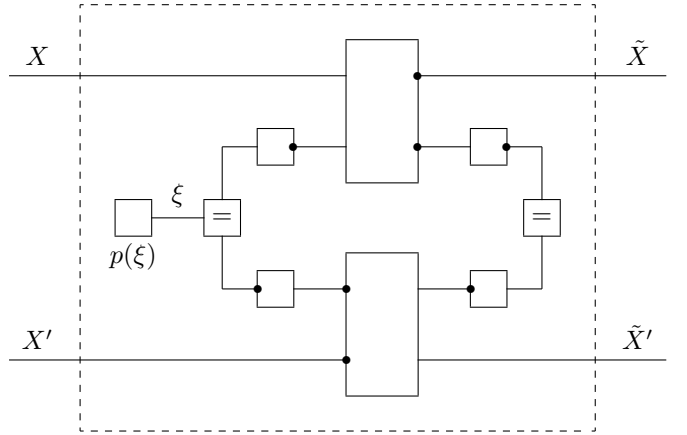


Fig. 45. Two quantum systems interact unitarily. (All unlabeled boxes are unitary matrices.) The resulting exterior function of the dashed box amounts to a measurement with unknown result.

and the factor  $f_\oplus$  in Fig. 43 is defined as

$$f_\oplus : \{0, 1\}^3 \rightarrow \{0, 1\} : \\ f_\oplus(\xi_1, \xi_2, \xi_3) \triangleq \begin{cases} 1, & \text{if } \xi_1 + \xi_2 + \xi_3 \text{ is even} \\ 0, & \text{otherwise.} \end{cases} \quad (52)$$

That Fig. 43 is a unitary matrix may be seen from Fig. 44.

Quantum circuits as in [12, Chap. 4] may then be viewed as, or are easily translated to, the upper half of factor graphs as in Fig. 36. (However, this upper half cannot, by itself, properly represent the joint probability distribution of several measurements.)

### C. Non-unitary Operators from Unitary Interactions

Up to now, we have considered systems composed from only two elements: unitary evolution and measurement. (The role and meaning of the latter continues to be debated, see also Section VI.) However, a natural additional element is shown in Fig. 45, where a primary quantum system interacts once with a secondary quantum system.

(The secondary quantum system might be a stray particle that arrives from “somewhere”, interacts with the primary system, and travels off to somewhere else. Or, with exchanged roles, the secondary system might be a measurement apparatus that interacts once with a particle of interest.)

Closing the dashed box in Fig. 45 does not, in general, result in a unitary operator. In fact, the situation of Fig. 45 may be viewed as a mixture of measurements as in Fig. 27: for any fixed  $\xi$ , Fig. 45 represents a measurement as in Fig. 27 except that the result of the measurement is ignored. In other words, marginalizing the secondary system away amounts to a measurement of the primary system (with unknown result).

It seems natural to conjecture that classicality emerges out of such interactions, as has been proposed by Zurek [23], [24] and others.

## VI. MEASUREMENTS RECONSIDERED

Our tour through quantum-mechanical concepts followed the traditional route where “measurement” is an unexplained primitive. However, progress has been made in understanding

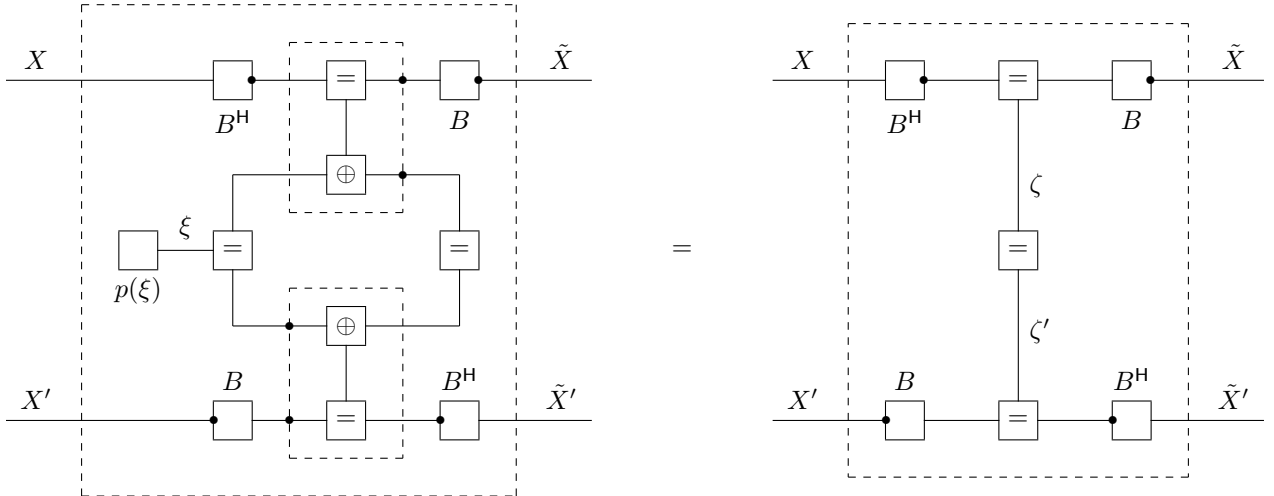


Fig. 46. Projection measurement (with unitary matrix  $B$ ) as marginalized unitary interaction. Left: unitary interaction as in Fig. 45; the inner dashed boxes are unitary (cf. Fig. 43). Right: resulting projection measurement (with unknown result  $\zeta$ ). The exterior functions left and right are equal.

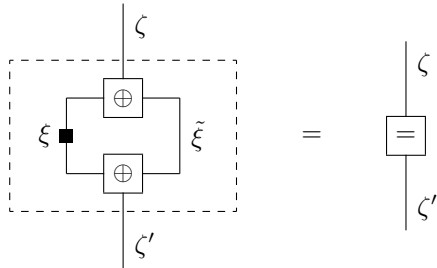


Fig. 47. Proof of the reduction in Fig. 46.

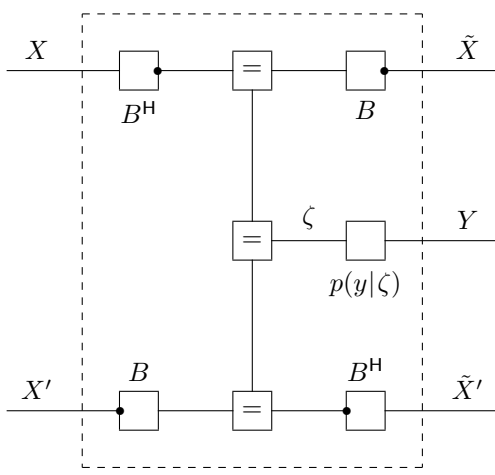


Fig. 48. Observing the post-measurement variable  $\zeta$  in Fig. 46 (right) via a (classical) ‘channel’  $p(y|\zeta)$ .

measurement as interaction [25], [26], essentially by reducing it to something like Fig. 45. There thus emerges a view of quantum-mechanical probabilities fundamentally involving only unitary transforms and marginalization. This view is still imperfectly developed (cf. [26]), but it is a fitting topic for the end of this paper.

### A. Projection Measurements

The realization of a projection measurement by a unitary interaction is exemplified in Fig. 46. As will be detailed below, Fig. 46 (left) is a unitary interaction as in Fig. 45 while Fig. 46 (right) is a projection measurement (with unknown result  $\zeta$ ). We will see that the exterior functions of Fig. 46 (left) and Fig. 46 (right) are equal.

All variables in Fig. 46 (left) take values in the set  $\{0, \dots, M-1\}$  (rather than in  $\{1, \dots, M\}$ ) and the box labeled “ $\oplus$ ” generalizes (52) to

$$f_{\oplus} : \{0, \dots, M-1\}^3 \rightarrow \{0, 1\} : \\ f_{\oplus}(\xi_1, \xi_2, \xi_3) \triangleq \begin{cases} 1, & \text{if } (\xi_1 + \xi_2 + \xi_3) \bmod M = 0 \\ 0, & \text{otherwise.} \end{cases} \quad (53)$$

We first note that the two inner dashed boxes in Fig. 46 (left) are unitary matrices, as is easily verified from Fig. 44. Therefore, Fig. 46 (left) is indeed a special case of Fig. 45.

The key step in the reduction of Fig. 46 (left) to Fig. 46 (right) is shown in Fig. 47, which in turn can be verified as follows: the product of the two factors in the box in Fig. 47 (left) is zero unless both

$$\xi + \zeta + \tilde{\xi} = 0 \pmod{M} \quad (54)$$

and

$$\xi + \zeta' + \tilde{\xi} = 0 \pmod{M}, \quad (55)$$

which is equivalent to  $\zeta = \zeta'$  and (54). For fixed  $\xi$  and  $\zeta$ , (54) allows only one value for  $\tilde{\xi}$ , which proves the reduction in Fig. 47.

The generalization from fixed  $\xi$  to arbitrary  $p(\xi)$  is straightforward.

We have thus established that the (marginalized) unitary interaction in Fig. 46 (left) acts like the projection measurement in Fig. 46 (right) and thereby creates the random variable  $\zeta$ .

Moreover, projection measurements are repeatable, i.e., repeating the same measurement (immediately after the first

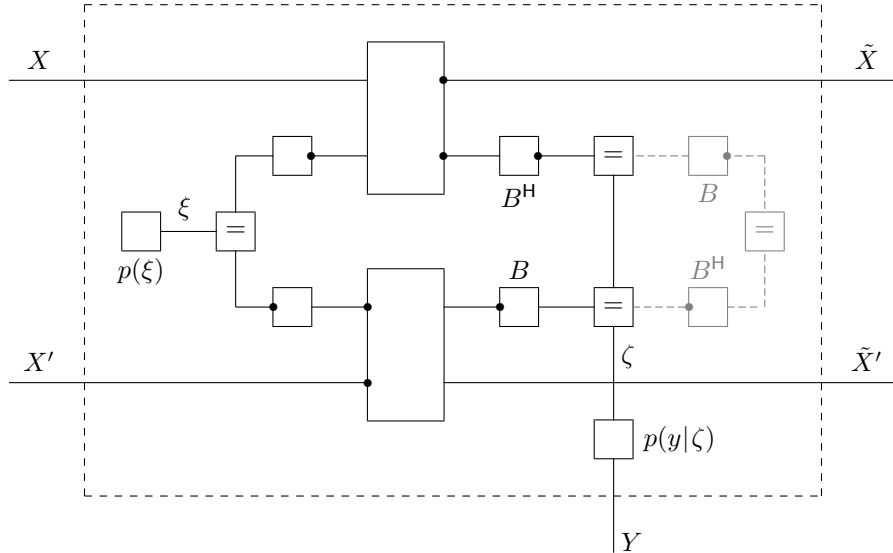


Fig. 49. General measurement as unitary interaction and marginalization. The matrix  $B$  and the unlabeled solid boxes are unitary matrices. The part with the dashed edges is redundant.

measurement) leaves the measured quantum system unchanged. (In fact, this property characterizes projection measurements.) Therefore, the random variable  $\zeta$  is an objective property of the quantum system after the measurement/interaction; it can be cloned, and it can, in principle, be observed via some “channel”  $p(y|\zeta)$ , as illustrated in Fig. 48.

The conditional-probability factor  $p(y|\zeta)$  allows, in particular, that  $\zeta$  is not fully observable because several values of  $\zeta$  lead to the same observation  $Y$ .

### B. General Measurements

A very general form of (indirect) measurement is shown in Fig. 49, which is identical to Fig. 45 except for the observable variable  $Y$ . The figure is meant to be interpreted as follows. Some primary quantum system (with variables  $X, X, \tilde{X}, \tilde{X}'$ ) interacts once with a secondary quantum system, which in turn is measured by a projection measurement as in Fig. 48. It is not difficult to verify (e.g., by adapting the procedure in [12, Box 8.1]) that an interaction as in Fig. 49 can realize any measurement as in Fig. 27.

## VII. MORE ABOUT RELATED WORK

Before we conclude, we offer some additional remarks on the prior literature.

### A. Tensor Networks

Various authors have used tensor networks (and related graphical notation) to represent the wave function  $|\Psi\rangle$  of several entangled spins at a given time. In general, the resulting states are called tensor network states (TNS), but depending on the structure of the tensor network, more specialized names like matrix product states (MPS), tree tensor states (TTS), etc., are used. A very nice overview of this line of work is given in the survey paper by Cirac and Verstraete [27], which also explains the connection of TNS to techniques like the

density matrix renormalization group (DMRG), the multiscale entanglement renormalization ansatz (MERA), and projected entangled pair states (PEPS).

If such tensor diagrams are used to represent quantities like  $\langle\Psi|\Psi\rangle$  or  $\langle\Psi|\sigma_2\sigma_4|\Psi\rangle$  (see, e.g., Fig. 2 in [27]), they have two conjugate parts, like the factor graphs in the present paper (Fig. 11 etc.).

The interested reader is also referred to [28], which represents various quantum mechanical concepts in terms of tensor networks.

### B. Quantum Bayesian Networks and Quantum Belief Propagation

Whereas the present paper uses conventional Forney factor graphs (with standard semantics and algorithms), various authors have proposed modified graphical models or specific “quantum algorithms” for quantum mechanical quantities [16], [29], [30]. Such graphical models (or algorithms) are not compatible with standard statistical models.

### C. Keldysh Formalism

There are some high-level similarities between the graphical models in the present paper and some diagrams that appear in the context of the Keldysh formalism (see, e.g., [31]); in particular, both have “two branches along the time axis.”

However, there are also substantial dissimilarities: first, the diagrams in the Keldysh formalism also have a third branch along the imaginary axis; second, our factor graphs are arguably more explicit than the diagrams in the Keldysh formalism.

### D. Normal Factor Graphs, Classical Analytical Mechanics, and Feynman Path Integrals

In [32], it is shown how Forney factor graphs (= normal factor graphs) can be used for computations in classical analytical mechanics. In particular, it is shown how to represent the

action  $S(x)$  of a trajectory  $x$  and how to use the stationary-sum algorithm for finding the path where the action is stationary.

It is straightforward to modify the factor graphs in [32] in order to compute, at least in principle, Feynman path integrals, where  $\exp(\frac{i}{\hbar}S(x))$  is integrated over a suitable domain of paths  $x$ : essentially by replacing the function nodes  $f(\cdot)$  in [32] by  $\exp(\frac{i}{\hbar}f(\cdot))$ , and by replacing the stationary-sum algorithm by standard sum-product message passing [4].

### VIII. CONCLUSION

We have proposed factor graphs for quantum-mechanical probabilities involving any number of measurements, both for basic projection measurements and for general measurements. Our factor graphs represent factorizations of complex valued functions  $q$  as in (3), of which all probabilities (and joint probabilities) are marginals. Therefore (and in contrast to other graphical representations of quantum mechanics), our factor graphs are fully compatible with standard statistical models. We also interpret a variety of concepts and quantities of quantum mechanics in terms of factorizations and marginals of such functions  $q$ .

In Appendix B, we point out that the factor graphs of this paper are amenable (at least in principle) to Monte Carlo algorithms. In Appendix A, we derive factor-graphs for the Wigner–Weyl representation of quantum probabilities.

We hope that our approach makes quantum-mechanical probabilities more accessible to non-physicists and further promotes the exchange of concepts and algorithms between physics and statistical inference that has been so fruitful in recent years [7].

### APPENDIX A WIGNER–WEYL REPRESENTATION

The Wigner–Weyl representation of quantum mechanics expresses the latter in terms of the “phase-space” coordinates  $\mathbf{q}$  and  $\mathbf{p}$  (corresponding to the position and the momentum, respectively, of classical mechanics). When transformed into this representation, the density matrix turns into a real-valued function.

So far in this paper, all variables were assumed to take values in some finite set without any structure. However, the Wigner–Weyl representation requires that both the original coordinates  $X$  and  $X'$  and the new coordinates  $\mathbf{p}$  and  $\mathbf{q}$  can be added and subtracted and admit a Fourier transform as in (59) and (63) below. In the following, we assume  $X_k, X'_k, \mathbf{p}_k, \mathbf{q}_k \in \mathbb{R}^N$  for all  $k$ .

In a factor graph with continuous variables, the exterior function of a box is defined by integrating over the internal variables, i.e., the sum in (5) and (6) is replaced by an integral. Moreover, the equality constraint function (9) becomes

$$f_=(x_1, \dots, x_n) = \delta(x_1 - x_2) \cdots \delta(x_{n-1} - x_n), \quad (56)$$

where  $\delta$  is the Dirac delta. Finally, matrices (cf. Section II-B) are generalized to operators, i.e., the sums in (11) and (12) are replaced by integrals.

The transformation to the Wigner–Weyl representation uses an operator  $W$  that will be described below. Factor graphs for

the Wigner–Weyl representation may then be obtained from the factor graphs in Sections III–V by a transformation as in Fig. 50. The example in this figure is a factor graph as in Fig. 23 with a single measurement, but the generalization to any number of measurements is obvious. Starting from the original factor graph (top in Fig. 50), we first insert neutral factors (identity operators) factored as  $I = WW^{-1}$  as shown in Fig. 50 (middle); clearly, this manipulation does not change  $p(y)$ . We then regroup the factors as in Fig. 50 (bottom), which again leaves  $p(y)$  unchanged. The Wigner–Weyl factor graph is then obtained by closing the dashed boxes in Fig. 50 (bottom). (The Wigner–Weyl representation has thus been obtained as a “holographic” factor graph transform as in [20], [21].)

The operator  $W$  encodes the relations

$$X = \mathbf{q} - \mathbf{s} \quad (57)$$

$$X' = \mathbf{q} + \mathbf{s} \quad (58)$$

and the Fourier transform with kernel

$$\mathcal{F}(\mathbf{s}, \mathbf{p}) = \left( \frac{1}{\pi\hbar} \right)^N e^{(i/\hbar)2\mathbf{p}^T \mathbf{s}}. \quad (59)$$

For the purpose of this paper,  $\hbar$  (the reduced Planck constant) is an arbitrary scale factor.

The factor-graph representation of the operator  $W$  (shown left in Fig. 51) consists of two factors: the first factor is

$$\delta(x - (\mathbf{q} - \mathbf{s})) \delta(x' - (\mathbf{q} + \mathbf{s})), \quad (60)$$

which encodes the constraints (57) and (58); the second factor is the Fourier kernel (59).

The factor-graph representation of  $W^{-1}$  (right in Fig. 51) consists of the inverse Fourier transform kernel

$$\mathcal{F}^{-1}(\mathbf{s}, \mathbf{p}) = e^{(-i/\hbar)2\mathbf{p}^T \mathbf{s}} \quad (61)$$

and the factor

$$\delta(\mathbf{q} - \frac{1}{2}(x + x')) \delta(\mathbf{s} - \frac{1}{2}(-x + x')). \quad (62)$$

Closing the “initial state” box in Fig. 50 yields the function

$$\mu_W(\mathbf{q}, \mathbf{p}) = \int_{-\infty}^{\infty} \left( \frac{1}{\pi\hbar} \right)^N e^{(i/\hbar)2\mathbf{p}^T \mathbf{s}} \rho(\mathbf{q} - \mathbf{s}, \mathbf{q} + \mathbf{s}) d\mathbf{s} \quad (63)$$

for  $\mathbf{q} = \mathbf{q}_0$  and  $\mathbf{p} = \mathbf{p}_0$ , which is easily seen to be real (since  $\rho(x, x') = \rho(x', x)$ ).

Closing the “termination” box in Fig. 50 yields the function

$$\begin{aligned} & \int_{-\infty}^{\infty} \int_{-\infty}^{\infty} \int_{-\infty}^{\infty} e^{(-i/\hbar)2\mathbf{p}^T \mathbf{s}} \delta(\mathbf{q} - \frac{1}{2}(x + x')) \\ & \quad \delta(\mathbf{s} - \frac{1}{2}(-x + x')) \delta(x - x') dx' dx d\mathbf{s} \\ & = \int_{-\infty}^{\infty} e^{(-i/\hbar)2\mathbf{p}^T \mathbf{s}} \delta(\mathbf{s}) d\mathbf{s} \end{aligned} \quad (64)$$

$$= 1. \quad (65)$$

The termination box thus reduces to an empty box and can be omitted.

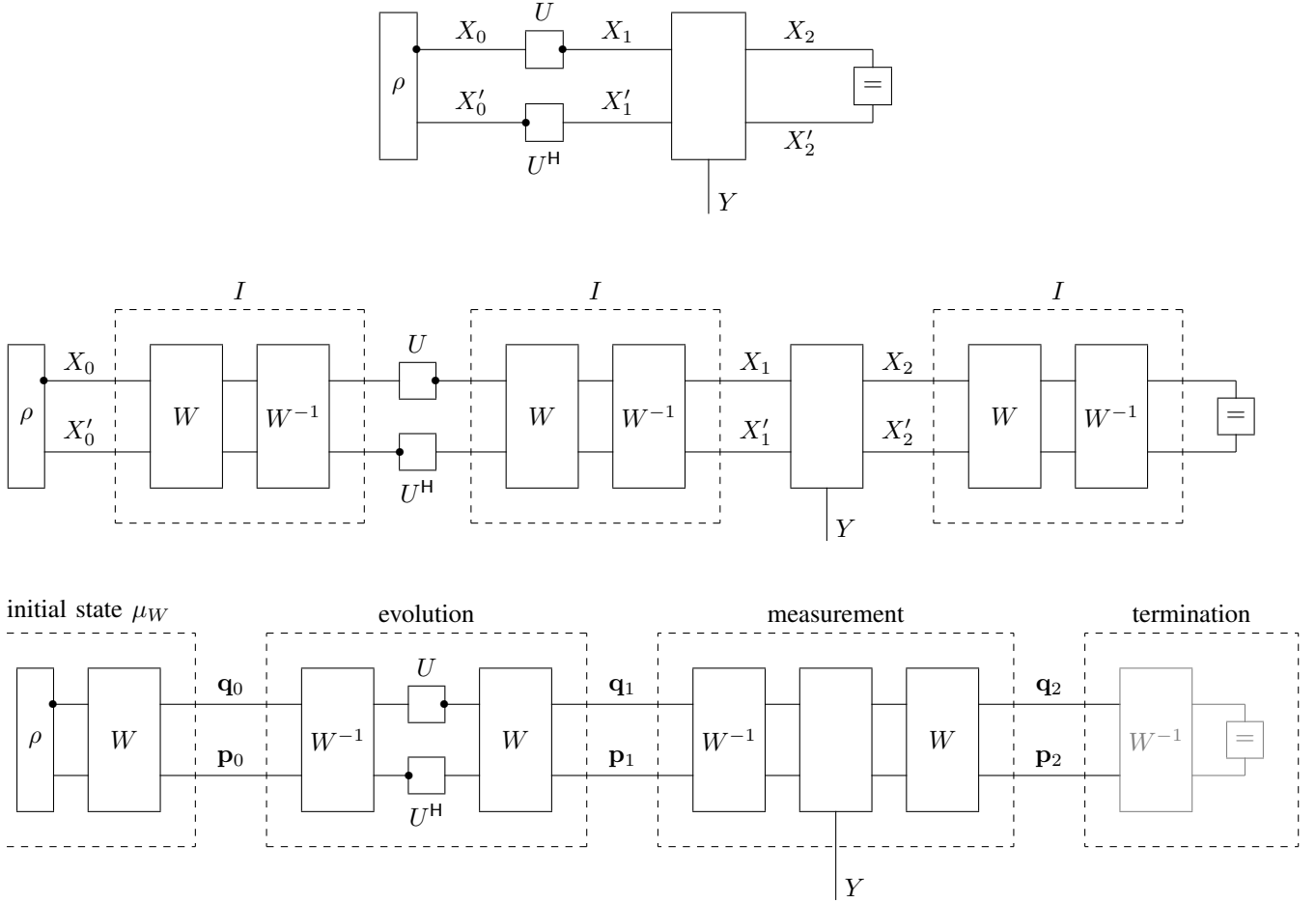


Fig. 50. Wigner-Weyl transform of a quantum factor graph with  $W$  as defined in Fig. 51. Top: quantum system with a single measurement yielding  $Y$ . Middle: inserting neutral factors (identity operators)  $I = WW^{-1}$  does not change the exterior function  $p(y)$ . Bottom: closing the dashed boxes yields the factor graph of the Wigner-Weyl representation. The termination box reduces to an empty box.

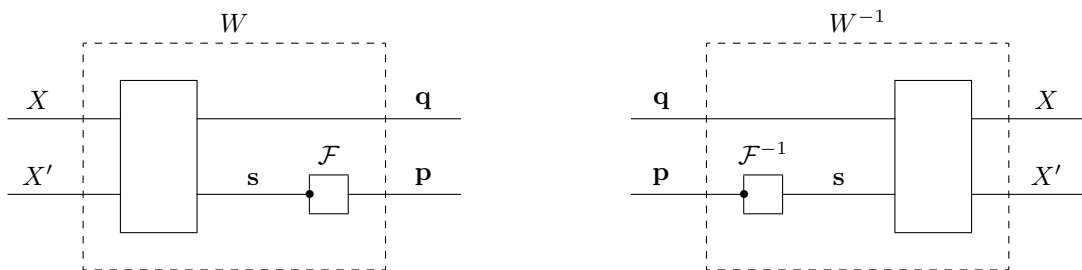


Fig. 51. Factor graphs of Wigner-Weyl transformation operator  $W$  (left) and its inverse (right). The unlabeled box inside  $W$  represents the factor (60); the unlabeled box inside  $W^{-1}$  represents the factor (62).

## APPENDIX B MONTE CARLO METHODS

Let  $f(x_1, \dots, x_n)$  be a nonnegative real function of finite-alphabet variables  $x_1, \dots, x_n$ . Many quantities of interest in statistical physics, information theory, and machine learning can be expressed as a partition sum

$$Z_f \triangleq \sum_{x_1, \dots, x_n} f(x_1, \dots, x_n) \quad (66)$$

of such a function  $f$ . The numerical computation of such quantities is often hard. When other methods fail, good results can sometimes be obtained by Monte Carlo methods [34]–[36]. A key quantity in such Monte Carlo methods is the probability mass function

$$p_f(x_1, \dots, x_n) \triangleq f(x_1, \dots, x_n)/Z_f. \quad (67)$$

An extension of such Monte Carlo methods to functions  $f$  that can be negative or complex was outlined in [37]. However, only the real case (where  $f$  can be negative) was addressed in some detail in [37]. We now substantiate the claim from [37] that complex functions  $q$  as represented by the factor graphs of this paper can be handled as in the real case.

We will use the abbreviation  $x \triangleq (x_1, \dots, x_n)$ , and, following [37], we define

$$Z_{|f|} \triangleq \sum_x |f(x)| \quad (68)$$

and the probability mass function

$$p_{|f|}(x) \triangleq \frac{|f(x)|}{Z_{|f|}} \quad (69)$$

Note that  $p_{|f|}$  inherits factorizations (and thus factor graphs) from  $f$ . This also applies to more general distributions of the form

$$p(x; \rho) \propto |f(x)|^\rho \quad (70)$$

for  $0 < \rho < 1$ .

For the real case, the gist of the Monte Carlo methods of [37] is as follows:

- 1) Generate a list of samples  $x^{(1)}, \dots, x^{(K)}$  either from  $p_{|f|}(x)$ , or from a uniform distribution over  $x$ , or from an auxiliary distribution  $p(x; \rho)$  as in (70).
- 2) Estimate  $Z$  (and various related quantities) from sums such as

$$\sum_{k: f(x^{(k)}) > 0} f(x^{(k)}) \quad (71)$$

and

$$\sum_{k: f(x^{(k)}) < 0} f(x^{(k)}), \quad (72)$$

or

$$\sum_{k: f(x^{(k)}) > 0} \frac{1}{f(x^{(k)})} \quad (73)$$

and

$$\sum_{k: f(x^{(k)}) < 0} \frac{1}{f(x^{(k)})}, \quad (74)$$

or, more generally,

$$\sum_{k: f(x^{(k)}) > 0} \frac{f(x^{(k)})^{\rho_1}}{f(x^{(k)})^{\rho_2}} \quad (75)$$

and

$$\sum_{k: f(x^{(k)}) < 0} \frac{f(x^{(k)})^{\rho_1}}{f(x^{(k)})^{\rho_2}} \quad (76)$$

The idea is always that the sampling probability equals the denominator (up to a scale factor), which results in simple expectations for these sums. (The quantities (75) and (76) are not actually mentioned in [37], but they arise from translating multi-temperature Monte Carlo methods (cf. [35], [36]) to the setting of [37].)

Note that Step 1 above (the generation of samples) generalizes immediately to the complex case; our issue here is Step 2, where the generalization is less obvious.

Recall now that all factor graphs in Sections III–V represent functions with the structure

$$q(x, x', y) = g(x, y) \overline{g(x', y)} \quad (77)$$

as in Fig. 11. But any such function satisfies

$$q(x, x', y) = \overline{q(x', x, y)}. \quad (78)$$

Under any of the probability distributions in Step 1 above, a configuration  $(x, x', y)$  then has the same probability as the conjugate configuration  $(x', x, y)$  (i.e.,  $(x, x', y)$  and  $(x', x, y)$  are so-called antithetic variates). We can thus double the list of samples in Step 1 by adding all the conjugate configurations. For the augmented list of samples, the sum (71) becomes

$$\sum_{k: f(x^{(k)}) + f(x^{(k)}) > 0} f(x^{(k)}) + \overline{f(x^{(k)})}, \quad (79)$$

and the sums (72)–(76) can be handled analogously.

## ACKNOWLEDGMENT

The material of this paper has been developing over a long time. Its beginnings have benefitted from discussions, mostly long ago, with Niclas Wiberg, Justin Dauwels, Frank Kschischang, and Nikolai Nefedov. More recently, we have profited from discussions with Ali Al-Bashabsheh, G. David Forney, Jr., and Yongyi Mao. We also thank the reviewers of [1] and Alexey Kovalev for pointing out pertinent work in the physics literature.

## REFERENCES

- [1] H.-A. Loeliger and P. O. Vontobel, “A factor-graph representation of probabilities in quantum mechanics,” *Proc. 2012 IEEE Int. Symp. on Information Theory*, Cambridge, MA, USA, July 1–6, 2012, pp. 656–660.
- [2] F. R. Kschischang, B. J. Frey, and H.-A. Loeliger, “Factor graphs and the sum-product algorithm,” *IEEE Trans. Inf. Theory*, vol. 47, pp. 498–519, Feb. 2001.
- [3] G. D. Forney, Jr., “Codes on graphs: normal realizations,” *IEEE Trans. Inf. Theory*, vol. 47, no. 2, pp. 520–548, 2001.
- [4] H.-A. Loeliger, “An introduction to factor graphs,” *IEEE Sig. Proc. Mag.*, Jan. 2004, pp. 28–41.
- [5] H.-A. Loeliger, J. Dauwels, Junli Hu, S. Krol, Li Ping, and F. R. Kschischang, “The factor graph approach to model-based signal processing,” *Proceedings of the IEEE*, vol. 95, no. 6, pp. 1295–1322, June 2007.

- [6] P. O. Vontobel and H.-A. Loeliger, "On factor graphs and electrical networks," in *Mathematical Systems Theory in Biology, Communication, Computation, and Finance*, J. Rosenthal and D. S. Gilliam, eds., IMA Volumes in Math. & Appl., Springer Verlag, 2003, pp. 469–492.
- [7] M. Mézard and A. Montanari, *Information, Physics, and Computation*. Oxford University Press, 2009.
- [8] M. I. Jordan, "Graphical models," *Statistical Science*, vol. 19, no. 1, pp. 140–155, 2004.
- [9] Ch. M. Bishop, *Pattern Recognition and Machine Learning*. New York: Springer Science+Business Media, 2006.
- [10] D. Koller and N. Friedman, *Probabilistic Graphical Models*. Cambridge, MA: MIT Press, 2009.
- [11] G. Auletta, M. Fortunato, and G. Parisi, *Quantum Mechanics*. Cambridge University Press, 2009.
- [12] M. A. Nielsen and I. L. Chuang, *Quantum Computation and Quantum Information*. Cambridge University Press, 2000.
- [13] M. Veltman, *Diagrammatica: The Path to Feynman Diagrams*. Cambridge Lecture Notes in Physics, 1994.
- [14] Z.-C. Gu, M. Levin, and X.-G. Wen, "Tensor-entanglement renormalization group approach as a unified method for symmetry breaking and topological phase transitions," *Phys. Rev. B*, vol. 78, p. 205116, Nov. 2008.
- [15] R. Mori, "Holographic transformation, belief propagation and loop calculus for generalized probabilistic theories," *Proc. 2015 IEEE Int. Symp. on Information Theory*, Hong Kong, China, June 14–19, 2015.
- [16] R. R. Tucci, "Quantum information theory – a quantum Bayesian net perspective," arXiv:quant-ph/9909039v1, 1999.
- [17] M. S. Leifer and D. Poulin, "Quantum graphical models and belief propagation," *Annals of Physics*, vol. 323, no. 8, pp. 1899–1946, Aug. 2008.
- [18] P. Cvitanović, *Group Theory: Birdtracks, Lie's, and Exceptional Groups*. Princeton Univ. Press, 2008.
- [19] E. Peterson, "Unshackling linear algebra from linear notation," arXiv:0910.1362, 2009.
- [20] A. Al-Bashabsheh and Y. Mao, "Normal factor graphs and holographic transformations," *IEEE Trans. Inf. Theory*, vol. 57, no. 2, pp. 752–763, Feb. 2011.
- [21] G. D. Forney, Jr., and P. O. Vontobel, "Partition functions of normal factor graphs," *Proc. Inf. Theory & Appl. Workshop*, UC San Diego, La Jolla, CA, USA, Feb. 6–11, 2011.
- [22] A. Al-Bashabsheh, Y. Mao, and P. O. Vontobel, "Normal factor graphs: a diagrammatic approach to linear algebra," *Proc. IEEE Int. Symp. Inf. Theory*, St. Petersburg, Russia, Jul. 31–Aug. 5, 2011, pp. 2178–2182.
- [23] W. H. Zurek, "Decoherence, einselection, and the quantum origins of the classical," *Rev. Mod. Phys.*, vol. 75, no. 3, pp. 715–775, July 2003.
- [24] W. H. Zurek, "Quantum Darwinism," *Nature Physics*, vol. 5, pp. 181–188, March 2009.
- [25] H.-P. Breuer and F. Petruccione, *Open Quantum Systems*. Oxford University Press, New York, NY, 2002.
- [26] M. Schlosshauer, "Decoherence, the measurement problem, and interpretations of quantum mechanics," *Rev. Mod. Phys.*, vol. 76, pp. 1267–1305, Oct. 2004.
- [27] J. I. Cirac and F. Verstraete, "Renormalization and tensor product states in spin chains and lattices," *J. Phys. A: Math. and Theor.*, vol. 42, no. 504004, pp. 1–34, 2009.
- [28] B. Coecke, "Quantum picturalism," *Contemporary Phys.*, vol. 51, no. 1, pp. 59–83, 2010.
- [29] M. G. Parker, "Quantum factor graphs," *Ann. Télécomm.*, vol. 56, no. 7–8, pp. 472–483, 2001.
- [30] M. S. Leifer, D. Poulin, "Quantum graphical models and belief propagation," *Ann. Phys.*, vol. 323, no. 8, pp. 1899–1946, 2008.
- [31] R. van Leeuwen, N. E. Dahlen, G. Stefanucci, C.-O. Almbladh, and U. van Barth, "Introduction to the Keldysh formalism," *Lect. Notes Phys.*, vol. 706, pp. 33–59, 2006.
- [32] P. O. Vontobel, "A factor-graph approach to Lagrangian and Hamiltonian dynamics," *Proc. IEEE Int. Symp. Information Theory*, St. Petersburg, Russia, Jul. 31 – Aug. 5, 2011, pp. 2183–2187.
- [33] R. P. Feynman and A. R. Hibbs, *Quantum Mechanics and Path Integrals*. New York: McGraw-Hill, 1965.
- [34] D. J. C. MacKay, "Introduction to Monte Carlo methods," in *Learning in Graphical Models*, M. I. Jordan, ed., Kluwer Academic Press, 1998, pp. 175–204.
- [35] R. M. Neal, *Probabilistic Inference Using Markov Chain Monte Carlo Methods*, Techn. Report CRG-TR-93-1, Dept. Comp. Science, Univ. of Toronto, Sept. 1993.
- [36] M. Molkaraie and H.-A. Loeliger, "Monte Carlo algorithms for the partition function and information rates of two-dimensional channels," *IEEE Trans. Inf. Theory*, vol. 59, no. 1, pp. 495–503, Jan. 2013.
- [37] M. Molkaraie and H.-A. Loeliger, "Extending Monte Carlo methods to factor graphs with negative and complex kernels," *Proc. 2012 IEEE Information Theory Workshop*, Lausanne, Switzerland, Sept. 3–7, 2012, pp. 367–371.